Electromagnetic structure of the helium isotopes*

J. S. McCarthy
Department of Physics, University of Virginia, Charlottesville, Virginia 22901
and High Energy Physics Laboratory, Stanford University, Stanford, California 94305

I. Sick†
Department of Physics, University of Basel, Basel, Switzerland
and High Energy Physics Laboratory, Stanford University, Stanford, California 94305

R. R. Whitney‡
High Energy Physics Laboratory, Stanford University, Stanford, California 94305
(Received 2 August 1976)

The elastic-electron scattering cross sections from ^{3}He and ^{4}He have been measured at incident electron energies between 170 and 750 MeV. Cross sections were separated into their longitudinal (charge) and transverse (magnetic) contributions using the Rosenbluth formula. Values of the ^{3}He charge form factor have been extracted to $q^2 = 20$ fm^{-2} and for the ^{3}He magnetic form factor to $q^2 = 16$ fm^{-2}. The ^{4}He form factor has been determined up to 6.2 fm^{-2}. Densities for the charge and magnetization have been deduced from phenomenological models used in a phase-shift solution of the Dirac equation. A model-independent determination of the nuclear densities has been performed in order to obtain realistic errors on the extracted distributions. After unfolding the nucleon size from the distributions the point density is shown to have a significant central depression for a radius <0.8 fm for both ^{3}He and ^{4}He. Comparison of the form factors is made with Faddeev and variational three-body calculations that use realistic two-body NN interactions. The influence of off-shell effects, three-body forces, meson-exchange corrections, and short-range correlations are discussed. At present no theoretical calculation that uses input derived entirely from nucleon-nucleon scattering is able to reproduce the experimental data.

[NUCLEAR REACTIONS ^{3,4}He(e,e'), $E=170$, 200, 250, 300, 350, 400, 450, 500, and 750 MeV; measured $\sigma(E,\theta)$. Measured charge form factor ^{3}He to $q^2=20$ fm^{-2} and magnetic form factor to $q^2=16$ fm^{-2}. Measured ^{4}He form factor to $q^2=6.2$ fm^{-2}. Deduced nuclear charge, magnetic and point-nucleon distributions from model-independent analysis.]

I. INTRODUCTION

Elastic electron scattering is an extremely useful experimental method for the quantitative study of nuclear structure. The interaction is completely described by quantum electrodynamics, and, moreover, the strength of the interaction is relatively weak. This permits a nondestructive investigation of nuclear systems and a quantitative description of the scattering process.

Advances in electron scattering techniques and facilities have increased the available maximum momentum transfer q, i.e., the lowest cross section ($\sim 10^{-37}$ cm^2/sr) that can be reached. We will emphasize the importance of obtaining cross sections at high q values since the spatial resolution of the "electron microscope" is directly proportional to the inverse momentum transfer; the minimal distance of resolution is $\sim 1.5/q_{\max}$. Another advantage of going to high q is the ability to measure Fourier components of the charge or magnetization density having very small amplitudes. This reduces the uncertainty involved in estimates of the higher frequency components that are not measured due to the finite $q_{\max}$.

The interest in the three-body nuclear systems stems from the fact that it is the simplest "nontrivial" nucleus that can be investigated by exact theoretical methods. The calculations based primarily upon either a Faddeev or variational method use the nucleon-nucleon force as the basic input. The ability to predict the three-body properties (binding energy, charge, and magnetic form factors) is one of the most stringent tests on the validity of the assumed nuclear force or the method of calculation.

The densities of the helium nuclei are also distinguished by extremely high values in the central region, higher than for any other nucleus. These nuclei are therefore expected to exhibit most strongly the effects of the short-range properties of the nuclear force. Details of the NN force not determined by NN scattering data may then become important. Isolation of contributions of a three-body force should also become easier when dealing with nuclei like ^{3}H or ^{3}He, since they are

tractable by exact theoretical methods. The interpretation of data in terms of *NN* forces becomes complicated by the fact that, at large q^2, the picture of a nucleus consisting of nucleons may no longer be applicable; in particular, the effect of meson degrees of freedom and possible isobar admixtures is still uncertain.

Previous experiments on ^{3}He and ^{3}H have been performed by Collard *et al.*[1] and extend to $q^2 = 8$ fm^{-2}. The cross sections as a function of q^2 showed very little structure and were not able to discriminate between different theoretical wave functions; the primary information that was necessary to reproduce the data was the rms radius. The ^{4}He nucleus had received considerable attention[2,3] before an intensive effort[4] resulted in the discovery of the diffraction minimum and secondary maximum extending to $q^2 = 20$ fm^{-2}. The first indication that the ^{4}He form factor deviated from a smooth Gaussian shape was furnished by the measurements of Repellin *et al.*[5]

Efforts were then instigated to also determine the more complex structure of ^{3}He by extending the measurements to high q, even though the existing data were entirely consistent with a continually decreasing form factor. In this paper we will present the final data of high momentum transfer scattering on ^{3}He, of which partial results were published earlier in Ref. 6.

II. EXPERIMENTAL PROCEDURE

The standard experimental arrangement for electron scattering at the Stanford High Energy Physics Laboratory was employed. For this experiment energies of 170, 200, 250, 300, 350, 400, 450, 500, and 750 MeV were used. A floating wire calibration for the nuclear magnetic resonance probe in the energy analyzing magnet gave the absolute energy to better than ±0.1%. The energy slit was set for 0.25% resolution in order to properly separate the elastic ^{3}He peak from the inelastic breakup at all energies. Using split secondary emission monitors (SEM) the beam position on the target was controlled to ±0.5 mm both left-right and up-down, and the spot size was less than 0.5 cm. Several fluorescent screens, which could be placed in the beam line and observed by remote TV, ensured that the beam was incident along the 0° line to within 0.02°.

The multiple scattering of electrons in the target was small enough so that the majority of electrons were collected in the Faraday cup, resulting in a total charge measurement for each data run. An integrating SEM upstream from the target was used to measure the (up to 5%) loss at the lowest energy, by comparing the target-in with the target-out collection efficiency of the Faraday cup.

Scattered electrons were observed by the 1.8 m spectrometer and 100 channel ladder detector.[7] The spectrometer has point-to-point focusing with a momentum acceptance of 7.5%. Entrance slits on the spectrometer determine the solid angle; $\Delta\theta$, the acceptance in the scattering plane, was always held at ±0.93°; $\Delta\phi$, the angle perpendicular to the scattering plane, was held at ±3.66° except for the 750 MeV data where it was reduced to ±2.60 to improve spectrometer energy resolution. The scattering angle is known to ±0.03°.

The focal plane detector has 100 plastic scintillator detectors located in the focal plane and 10 liquid Čerenkov detectors as backing counters. A fast coincidence is required between a plastic scintillator detector and the appropriate liquid Čerenkov detector. The average momentum acceptance of each plastic scintillator detector (channel) is 0.075%. Together with a heavy shielding of the focal plane, this system ensures elimination of background even for the lowest cross sections measured.

For a given data run, all relevant parameters were entered into the on-line IBM 7700 data acquisition system. Before a cross section could be computed, several corrections had to be made. A counting rate correction computed from the counts per channel and number of beam pulses in a run was applied to account for the dead time. The beam current was always kept low enough so that this correction was never more than 4% and usually less than 1%.

The dead-time corrected counts in every channel were then divided by the relative efficiencies of the various channels. Prior data runs, at several spectrometer settings on the quasielastic peak of a heavy nucleus, were used to compute the relative efficiencies. The quasielastic peak as a function of energy loss of the scattered electron was fitted by a polynomial. The fit was made to several overlapping spectra, and a channel's deviation from the fit gave the relative efficiency for that channel.

The differential cross section was then corrected for the overall system efficiency. For this experiment the system efficiency was determined at incident energies of 200, 250, 400, and 550 MeV. Cross sections for elastic scattering off the proton were measured using a CH_2 and C target. The proton cross sections were normalized to the absolute proton cross sections as measured by Janssens *et al.*[8] The uncertainty in the overall system efficiency is ±2% (better at low q) and mainly due to the uncertainty in the absolute proton cross sections. The proton cross sections and relative

efficiencies were taken during the two days prior to the start of the ^{3}He and ^{4}He measurements. During the course of the experiment, the stability of the ^{3}He cross sections being measured was checked by remeasuring the ^{4}He cross sections. Because of its small change in density with temperature and high thermal conductivity, the superfluid ^{4}He makes a very stable target. No change in the system efficiency was observed within the statistics of the measurements.

Because aluminum windows hold the liquid ^{3}He and ^{4}He, an additional correction was required. At each energy and angle a spectrum was also taken from an empty target which had windows only. Depending on the kinematics, the aluminum spectra were shifted up to 1.7 channels to correct for differences in the scattered electron's ionization loss in helium. The statistics of the aluminum subtractions was included in the errors for the data points. In the diffraction minimum the background statistical errors were as large as the error due to the counting statistics in the elastic peaks.

Liquid target Dewar

While using incident electrons of several hundred MeV the important criteria for a ^{3}He target are to achieve the maximum desired target density and thickness while, at the same time, having a minimum amount of window material in the beam.

The first ^{3}He targets consisted of stainless-steel cylinders containing pressurized gas at room temperature.[1] Pressures of up to 200 atm were used, and window thicknesses, dependent on the scattering angle, were approximately 0.6 g/cm^2 or 0.045 radiation lengths.

Previous to this experiment one liquid ^{3}He target[9] had been used for high energy electron scattering. In that case, the heat deposited in the liquid ^{3}He was removed by pumping on its own

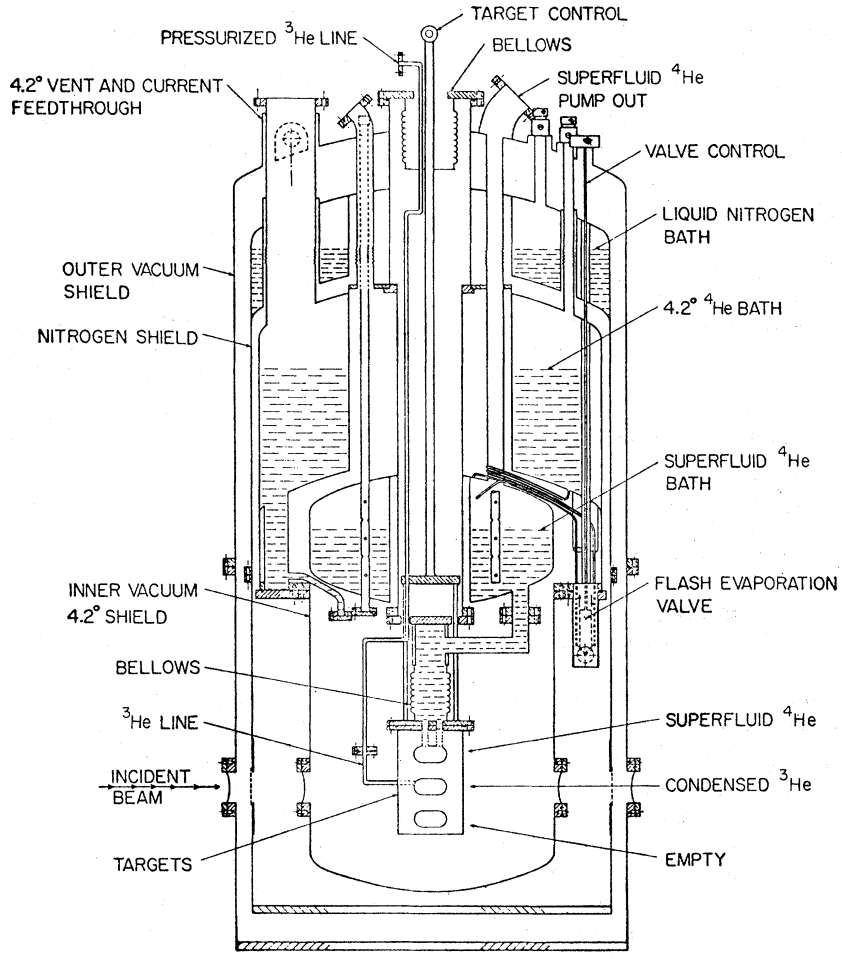

FIG. 1. Cryogenic target Dewar.

vapor. The maximum average beam current that could be tolerated without bubbling was 0.01 μA, far below the 1 μA average beam current of the Mark III accelerator. For the present experiment, the liquid ^{3}He was to be in thermal contact with a liquid ^{4}He bath (pumped below the ^{3}He critical temperature of 3.3 K); this ^{4}He bath can be held quite stable and permits the removal of heat deposition of the order of watts.

The design of the new liquid target Dewar was based on our experience with the liquid ^{4}He target,[4] liquid ^{3}He target, and a ^{3}He-^{4}He dilution refrigerator system.[10] Provision was made so that the Dewar (60 cm in diameter) could accommodate a ^{3}He-^{4}He dilution refrigerator and also a large superconducting magnet for possible future experiments. A schematic view of the liquid target Dewar[11] is shown in Fig. 1.

The vacuum container as well as the nitrogen and inner vacuum shield has three windows, each subtending an angular range of 100°. The Al windows are 5 cm high and have thicknesses of 30, 15, and 7 mg/cm^2, respectively. The flanges holding these windows can be rotated in increments of 10° relative to the top of the Dewar. The outer and inner heat shields are connected to the liquid nitrogen and liquid helium baths. At a number of points temperature and liquid level are monitored by measuring the resistance of Spear grade 1002, 200 Ω resistors using an ac resistance bridge.

The 15 liter superfluid ^{4}He bath and the targets have a separate inner vacuum. The cool-down and removal of the heat deposited by the beam is achieved by pumping on the superfluid ^{4}He bath (average vapor pressure ~0.2 atm). Continuous refilling of the superfluid ^{4}He bath can be performed by using the flash evaporation valve.

The closed-circuit ^{3}He system includes a 28 liter storage tank containing 17 liter STP of ^{3}He. A 6 liter ballast tank was used to stabilize the ^{3}He pressure when the target was filled and to collect the ^{3}He gas in case of a sudden warm-up of the target. The ^{3}He was transferred to the target through an activated charcoal trap at liquid nitrogen temperature, and impurities in the ^{3}He were removed. To empty the target, an Edwards ED-500 sealed rotary pump was used.

The ^{3}He target was filled to a level well above the level of the superfluid ^{4}He bath. In this situation, the ^{3}He liquid-gas interface is at a higher temperature than the target liquid, and the target liquid operates at a pressure higher than the one corresponding to the equilibrium point. As compared with the partially filled target, bubbling of the ^{3}He then occurred at a beam current of 1.5 μA rather than 0.4 μA.

Because liquid ^{3}He is slightly compressible, the effective target thickness depends not only on the temperature but also on the pressure.[12] Figure 2 gives the ^{3}He effective target thickness vs the superfluid ^{4}He bath pressure (which is a function of the temperature) for several ^{3}He pressures in the range used in the range used in this experiment. The density of the superfluid ^{4}He is known to be 0.1454 g/cm^3 and changes less than 0.1% in the range of pressures used.

In order to get the target thickness in mg/cm^2, the physical thickness of the target must be determined. At room temperature both the ^{3}He and ^{4}He cells had a thickness of 1.435 ± 0.002 cm. The copper block was 1.285 cm thick, the aluminum windows bulging out an additional 0.075 cm on average. An accurate direct low temperature measurement of the thickness could not be made without endangering the aluminum windows. The parameters for the contraction of aluminum and copper with temperature are known so that the low temperature thickness could be calculated. The largest uncertainty of ±1% comes from the amount that the windows are pushed out by the liquids in the cell. The calculation gave a thickness of 1.318 ± 0.015 cm.

As will be discussed in the next chapter the thickness used in the analysis was checked by comparing the low-momentum transfer 200 MeV data to the Darmstadt ^{4}He data which was measured using a gaseous ^{4}He-H_2 mixture.[2] The resultant thickness in this analysis was 1.328 ± 0.01 cm (ignoring the possible error in the absolute hydrogen calibration for the Darmstadt data).

The ^{3}He liquid in the volume of the beam can be at a higher temperature than the surrounding ^{3}He liquid. Also, the average temperature of the

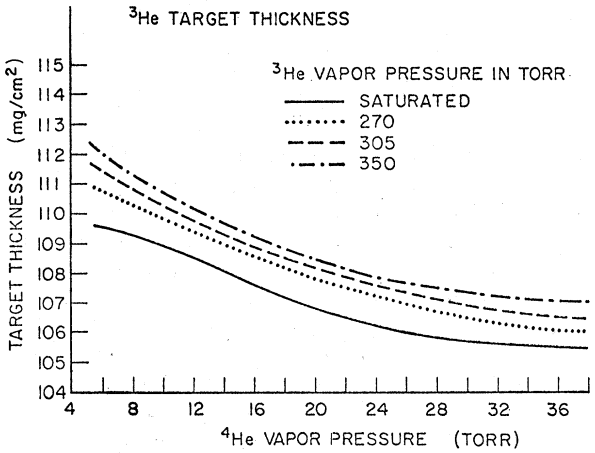

FIG. 2. ^{3}He target thickness as a function of ^{4}He vapor pressure (temperature).

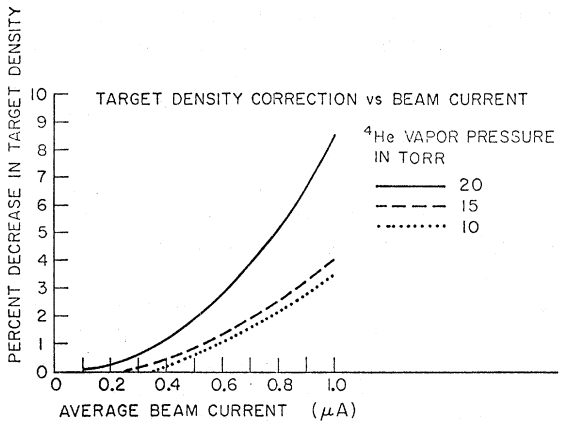

FIG. 3. Corrections to ^{3}He target density as function of beam current.

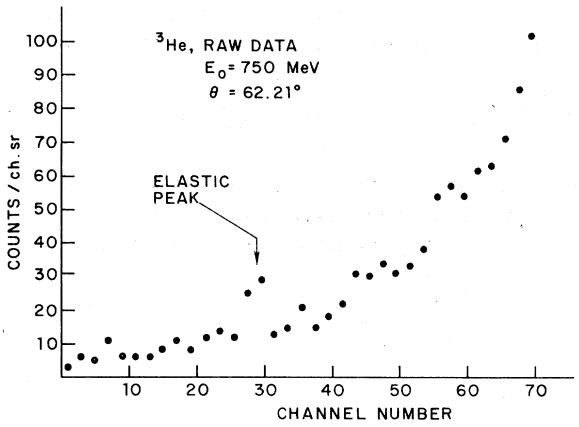

FIG. 5. Spectra of electrons scattered from ^{3}He, before subtraction of window-contribution and radiative effects.

liquid ^{3}He, as monitored by the gas pressure, could be as much as 0.2° higher in temperature than the copper block when the beam current was near 1 μA. The procedure to determine the ^{3}He target density was to measure cross sections at a fixed energy and angle while varying the incident beam current (Fig. 3). During the experiment the beam current and target temperature were kept in a region giving less than a 2% correction, except for very low cross sections where the statistical errors were large.

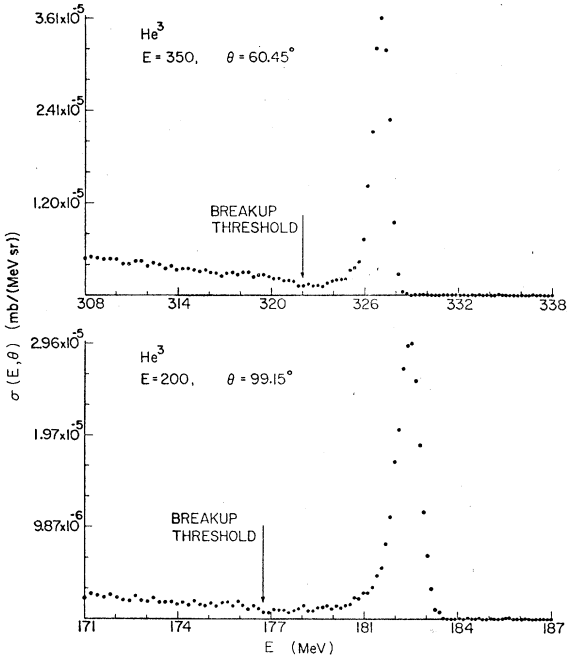

FIG. 4. Spectra of electrons scattered from ^{3}He, before radiative unfolding.

III. DATA REDUCTION AND RESULTS

Spectra of scattered electrons from ^{3}He are shown in Figs. 4 and 5. The measured scattering cross sections were corrected for the various radiative effects.[14,15] The radiative-corrected cross sections then were separated into longitudinal (charge) and transverse (magnetic) contributions. The relationship between the measured differential cross sections, $d\sigma/d\Omega$, and the properties of the ^{3}He nucleus is easily understood when using plane wave Born approximation (one photon exchange). From the elastic cross sections the scattering from a point charge and magnetic moment are factored out; the quantity remaining is defined as $F_{exp}(q^2, \theta)$. By plotting the form factor at constant q as a function of θ, one separates out the two physical form factors $F_{ch}(q^2)$ and $F_{mag}(q^2)$ (Fig. 6).

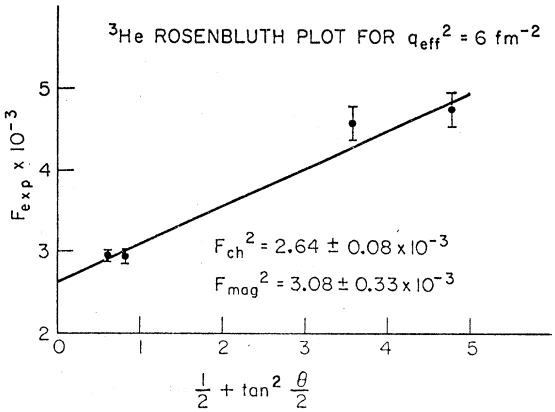

FIG. 6. Rosenbluth plot for ^{3}He.

In Born approximation the differential scattering cross section from the spin $-\frac{1}{2}$ ^{3}He nucleus, with anomalous magnetic moment K, charge Ze, and mass M, can be represented as follows (where $h=c=1$):

$$\frac{d\sigma}{d\Omega}=\left(\frac{Z\alpha}{2E}\right)^2\frac{\cos^2\frac{1}{2}\theta}{\sin^4\frac{1}{2}\theta[1+(2E/M)\sin^2\frac{1}{2}\theta]}\frac{1}{1+q^2/4M^2}\{F_{ch}{}^2(q)+F_{mag}{}^2(q)(1+K)^2\frac{q^2}{4M^2}[1+2(1+q^2/4M^2)\tan^2\tfrac{1}{2}\theta]\}. \quad (1)$$

The small effects of Coulomb distortion can approximately be taken into account if F_{ch} and F_{mag} are separated by values of q_{eff} rather than q, where

$$q_{eff}=q\left(1+\frac{4}{3}\frac{Z\alpha}{r_{eq}E_{c.m.}}\right), \quad (2)$$

$$E_{c.m.}=\frac{1}{1+(2E/M)}. \quad (3)$$

This correction becomes visible only near diffraction minima, the position of which will occur at the same value of q_{eff} (but not q) when cross sections are measured at different incident energies.

A check of the procedure was carried out systematically by scattering from ^{4}He where no magnetic contribution should occur. If the corrected q_{eff} was not used in the Rosenbluth plots, a small nonzero value for the magnetic scattering could be observed. The validity of the Born approximation for $Z=2$ is also proven by an analysis of the ^{4}He data, which also have been fitted by using a phase-shift code. In this case the cross sections are obtained by solving the Dirac equation for the phase shift of each partial wave for electrons scattered by a phenomenological central charge density. Within experimental uncertainties the identical charge densities have been found when using the phase-shift code or the plane wave Born approximation (PWBA).

^{3}He magnetic data were separated using the Born approximation as described above; a representative plot is shown in Fig. 6. In this region of q the charge scattering dominated the measured cross section and the charge cross section was obtained by correcting the total cross section for the measured percentage of magnetic scattering.

The absolute value of the extracted form factors depends critically upon the liquid target thickness. The low-q results of Ref. 2 on ^{4}He were used to check the consistency of our measurements. Our measurements of the cross section agree very well with those of Ref. 2 in the same region of momentum transfer and this confirms that our target thickness is known to better than 1.5%.

The final values of the form factors are presented in Tables I–III. In the region where the data overlap, the experimental values for the charge form factor of ^{3}He agree with the previous results of Collard *et al.*[1] The same is true for ^{4}He, where we find excellent agreement with the data of Refs. 2 and 4.

TABLE I. ^{3}He charge form factors.

q^2	$F_{ch}{}^2$	q^2	$F_{ch}{}^2$
0.347	$(6.82\pm0.17)\times10^{-1}$	3.50	$(2.72\pm0.09)\times10^{-2}$
0.400	$(6.51\pm0.16)\times10^{-1}$	4.00	$(1.70\pm0.06)\times10^{-2}$
0.451	$(6.02\pm0.15)\times10^{-1}$	4.50	$(1.08\pm0.05)\times10^{-2}$
0.500	$(5.82\pm0.15)\times10^{-1}$	5.00	$(6.76\pm0.23)\times10^{-3}$
0.542	$(5.48\pm0.14)\times10^{-1}$	5.50	$(4.07\pm0.14)\times10^{-3}$
0.600	$(5.16\pm0.13)\times10^{-1}$	6.00	$(2.64\pm0.08)\times10^{-3}$
0.639	$(4.87\pm0.12)\times10^{-1}$	6.50	$(1.67\pm0.10)\times10^{-3}$
0.700	$(4.55\pm0.11)\times10^{-1}$	7.00	$(1.05\pm0.06)\times10^{-3}$
0.800	$(4.26\pm0.11)\times10^{-1}$	7.50	$(6.61\pm0.80)\times10^{-4}$
0.900	$(3.85\pm0.10)\times10^{-1}$	8.00	$(4.09\pm0.59)\times10^{-4}$
1.000	$(3.32\pm0.08)\times10^{-1}$	9.00	$(1.69\pm0.39)\times10^{-4}$
1.100	$(2.97\pm0.08)\times10^{-1}$	9.50	$(1.07\pm0.34)\times10^{-4}$
1.200	$(2.69\pm0.07)\times10^{-1}$	10.00	$(3.75\pm3.15)\times10^{-5}$
1.500	$(1.93\pm0.05)\times10^{-1}$	11.00	$(0.0+2.29,-0.00)\times10^{-5}$
1.800	$(1.39\pm0.04)\times10^{-1}$	11.50	$(3.6+15,-3.6)\times10^{-6}$
2.000	$(1.15\pm0.03)\times10^{-1}$	12.50	$(0.0+1.5,-0.0)\times10^{-5}$
2.20	$(9.43\pm0.24)\times10^{-2}$	13.50	$(2.55\pm0.91)\times10^{-5}$
2.50	$(6.91\pm0.18)\times10^{-2}$	14.00	$(4.95\pm1.62)\times10^{-5}$
2.70	$(5.71\pm0.17)\times10^{-2}$	16.00	$(3.05\pm0.62)\times10^{-5}$
2.80	$(4.94\pm0.16)\times10^{-2}$	18.00	$(3.51\pm0.99)\times10^{-5}$
3.00	$(4.19\pm0.11)\times10^{-2}$	20.00	$(3.06\pm0.64)\times10^{-5}$

TABLE II. ^{3}He magnetic form factors.

q^2	F_m^2	q^2	F_m^2
2.00	$(1.03 \pm 0.35) \times 10^{-1}$	7.50	$(1.06 \pm 0.46) \times 10^{-3}$
2.80	$(4.90 \pm 0.97) \times 10^{-2}$	8.00	$(3.80 \pm 3.13) \times 10^{-4}$
3.00	$(3.88 \pm 0.35) \times 10^{-2}$	9.00	$(2.04 \pm 1.53) \times 10^{-4}$
3.50	$(1.42 \pm 0.85) \times 10^{-2}$	9.50	$(1.20 \pm 1.18) \times 10^{-4}$
4.00	$(1.39 \pm 0.36) \times 10^{-2}$	10.00	$(1.93 \pm 1.05) \times 10^{-4}$
4.50	$(1.04 \pm 0.13) \times 10^{-2}$	11.00	$(1.46 \pm 0.73) \times 10^{-4}$
5.00	$(5.28 \pm 1.57) \times 10^{-3}$	11.50	$(5.66 \pm 4.71) \times 10^{-5}$
5.50	$(5.56 \pm 0.85) \times 10^{-3}$	12.50	$(4.2 + 5.3, -4.2) \times 10^{-5}$
6.00	$(3.07 \pm 0.33) \times 10^{-3}$	14.00	$(0.5 + 0.9, -0.5) \times 10^{-5}$
6.50	$(2.13 \pm 0.69) \times 10^{-3}$	16.00	$(0.3 + 0.7, -0.3) \times 10^{-5}$
7.00	$(1.29 \pm 0.39) \times 10^{-3}$		

For the ^{3}He magnetic form factor, this experiment agrees with the 180° data of Ref. 13, but disagrees somewhat with the results of Ref. 1. This experiment had been performed with similar equipment as used for the present one, but with an energy resolution that did not allow proper separation of elastic and breakup contributions. The determination of the magnetic form factor is particularly sensitive to the angular dependence as function of energy, and a small breakup contribution can have a significant effect. In the present experiment such inelastic contributions to the elastic cross section do not occur.

IV. DATA ANALYSIS

A. Model densities

In this section the distributions of magnetic moment and charge are derived. The former is obtained using PWBA, the latter by employing PWBA or the exact phase-shift calculation. Corrections to this type of analysis concern intermediate excitation of the nuclear system (dispersion corrections) and the nonrelativistic reduction of the measured form factor. We will discuss the effects of these corrections later in this section; it will be shown that they are very small. In the following analysis, the nuclear recoil in the Born-approximation matrix element has been neglected and the partial-wave analysis in the phase-shift calculation has been performed in the center-of-momentum frame.

The charge and magnetic form factor were first analyzed in terms of phenomenological models for the densities. In Born approximation the form factor is given as the Fourier-Bessel transform

$$F(q) = \frac{1}{Ze} \int_0^\infty \frac{\sin(qr)}{qr} \rho(r) 4\pi r^2 \, dr \tag{4}$$

of the charge or magnetization density. The magnetization density $\mu(r)$ is normalized such that $\int \mu(r) d^3r = \mu_{^3\mathrm{He}}$.

The basic distribution used to fit the ^{3}He charge and magnetic distribution is given by

$$\rho_0(r) = \frac{Z}{8\pi^{3/2}} \left[\frac{1}{a^3} e^{-r^2/4a^2} - \frac{b^2(6c^2 - r^2)}{4c^7} e^{-r^2/4c^2} \right]. \tag{5}$$

This density corresponds to a form factor

$$F_0(q) = e^{-a^2q^2} - b^2q^2 e^{-c^2q^2}. \tag{6}$$

This distribution gives an excellent fit to the ^{3}He charge form factor out to $q^2 = 8$ fm^{-2}, and to the magnetic data to the maximum measured value at

TABLE III. ^{4}He form factors.

q^2	F_{ch}^2	q^2	F_{ch}^2
0.348	$(7.21 \pm 0.18) \times 10^{-1}$	1.817	$(1.88 \pm 0.04) \times 10^{-1}$
0.401	$(6.87 \pm 0.10) \times 10^{-1}$	2.015	$(1.56 \pm 0.04) \times 10^{-1}$
0.452	$(6.53 \pm 0.12) \times 10^{-1}$	2.020	$(1.59 \pm 0.03) \times 10^{-1}$
0.502	$(6.29 \pm 0.12) \times 10^{-1}$	2.224	$(1.32 \pm 0.02) \times 10^{-1}$
0.544	$(6.09 \pm 0.15) \times 10^{-1}$	2.521	$(1.01 \pm 0.03) \times 10^{-1}$
0.603	$(5.76 \pm 0.10) \times 10^{-1}$	2.53	$(9.85 \pm 0.19) \times 10^{-2}$
0.642	$(5.50 \pm 0.14) \times 10^{-1}$	2.55	$(9.67 \pm 0.24) \times 10^{-2}$
0.704	$(5.23 \pm 0.09) \times 10^{-1}$	2.65	$(8.83 \pm 0.22) \times 10^{-2}$
0.747	$(4.91 \pm 0.12) \times 10^{-1}$	2.76	$(8.18 \pm 0.20) \times 10^{-2}$
0.805	$(4.74 \pm 0.09) \times 10^{-1}$	2.87	$(7.34 \pm 0.18) \times 10^{-2}$
0.856	$(4.51 \pm 0.11) \times 10^{-1}$	3.03	$(6.22 \pm 0.10) \times 10^{-2}$
0.907	$(4.30 \pm 0.08) \times 10^{-1}$	3.05	$(6.28 \pm 0.12) \times 10^{-2}$
1.005	$(4.02 \pm 0.08) \times 10^{-1}$	3.08	$(5.99 \pm 0.15) \times 10^{-2}$
1.009	$(3.91 \pm 0.10) \times 10^{-1}$	3.54	$(3.86 \pm 0.08) \times 10^{-2}$
1.107	$(3.69 \pm 0.08) \times 10^{-1}$	3.85	$(2.93 \pm 0.07) \times 10^{-2}$
1.110	$(3.56 \pm 0.09) \times 10^{-1}$	4.06	$(2.48 \pm 0.05) \times 10^{-2}$
1.208	$(3.34 \pm 0.07) \times 10^{-1}$	4.11	$(2.30 \pm 0.06) \times 10^{-2}$
1.212	$(3.28 \pm 0.06) \times 10^{-1}$	4.32	$(1.91 \pm 0.05) \times 10^{-2}$
1.315	$(2.92 \pm 0.07) \times 10^{-1}$	4.64	$(1.40 \pm 0.03) \times 10^{-2}$
1.417	$(2.68 \pm 0.07) \times 10^{-1}$	5.06	$(9.87 \pm 0.25) \times 10^{-3}$
1.511	$(2.52 \pm 0.04) \times 10^{-1}$	6.08	$(3.59 \pm 0.07) \times 10^{-3}$
1.519	$(2.45 \pm 0.06) \times 10^{-1}$	6.13	$(3.22 \pm 0.11) \times 10^{-3}$
1.622	$(2.26 \pm 0.06) \times 10^{-1}$	6.22	$(2.78 \pm 0.14) \times 10^{-3}$
1.725	$(2.05 \pm 0.05) \times 10^{-1}$		

$q^2 = 12.5$ fm^{-2}. To reproduce the diffraction minimum in the ^{3}He charge form factor, it was necessary to add a modification, $\Delta\rho(r)$, to the charge density:

$$\Delta\rho(r) = \frac{Zpdq_0^2}{2\pi^{3/2}}\left[\frac{\sin(q_0 r)}{q_0 r} + \frac{p^2}{2q_0^2}\cos(q_0 r)\right] e^{-p^2r^2/4} \tag{7}$$

which corresponds to a form factor change of

$$\Delta F(q) = de^{-[(q-q_0)/p]^2} . \tag{8}$$

The experimental form factors and the best fit curve (obtained by phase-shift calculation) are shown in Fig. 7. The curve has been folded with spectrometer solid angle acceptance. The best fit charge distribution, $\rho(r) = \rho_0(r) + \Delta\rho(r)$, is shown in Fig. 8. The χ^2 per degree of freedom is 0.7. The best fit values for the parameters of ^{3}He charge distribution are $a = 0.675 \pm 0.008$ fm, $b = 0.366 \pm 0.025$ fm, $c = 0.836 \pm 0.032$ fm, $d = (-6.78 \pm 0.83) \times 10^{-3}$, $p = 0.90 \pm 0.16$ fm^{-1}, and $q_0 = 3.98 \pm 0.09$ fm^{-1}.

The diffraction minimum in the ^{3}He charge form factor fit occurs at $q^2 = 11.6$ fm^{-2} and the root mean square radius of the distribution is $r_{\rm rms} = 1.88 \pm 0.05$ fm.

The best fit parameters for the ^{3}He magnetic distribution are $a = 0.654 \pm 0.024$ fm, $b = 0.456 \pm 0.029$ fm, and $c = 0.821 \pm 0.053$ fm.

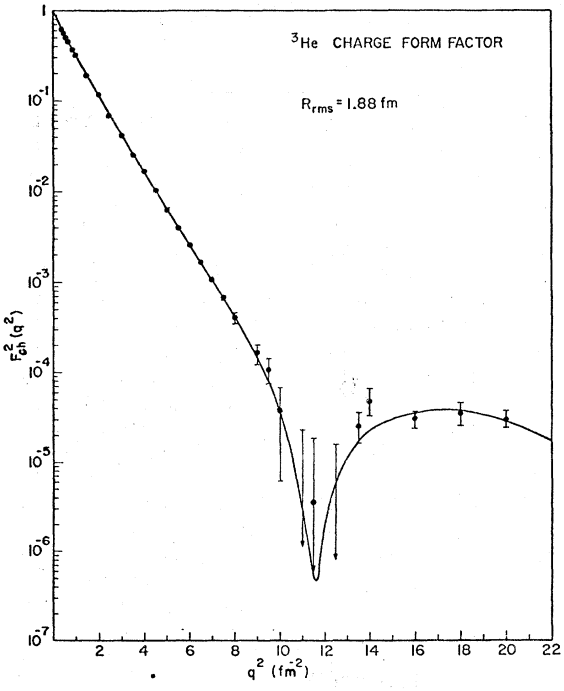

FIG. 7. ^{3}He charge form factors together with phenomenological fit [Eqs. (6) and (7)].

The experimental ^{3}He magnetic form factors and best fit curve are shown in Fig. 9. The root mean square radius is $r_{\rm rms} = 1.95 \pm 0.11$ fm. The χ^2 per degree of freedom is 0.9.

The ^{4}He data were fitted with the two charge distributions used earlier in Ref. 4. The three-parameter Fermi density

$$\rho(r) = \frac{\rho_0[1 + \omega(r^2/c^2)]}{1 + e^{(r-c)/z}} \tag{9}$$

was used as well as the form factor

$$F(q) = [1 - (a^2q^2)^6]e^{-b^2q^2} \tag{10}$$

which corresponds to a lengthy expression for $\rho(r)$ listed in Ref. 4.

The best fit parameters for the three-parameter Fermi distribution are $w = 0.517 \pm 0.016$, $c = 0.964 \pm 0.012$, and $z = 0.322 \pm 0.007$ fm.

The $r_{\rm rms}$ is 1.71 fm, the χ^2 per degree of freedom is 0.8. The best fit parameters for the second distribution are $a = 0.316$ fm and $b = 0.675$ fm. The best fit value of $r_{\rm rms}$ is 1.65 ± 0.04 fm, the χ^2 per degree of freedom is 0.7. The results for the ^{4}He form factor using the three-parameter Fermi distribution are shown in Fig. 10. These results are in excellent agreement with those of Ref. 4. Due to the smaller uncertainties of the present ^{4}He data, the charge density derived from the combined set of data is determined with considerably smaller uncertainties.

One notes that the two charge distributions for ^{4}He give slightly different $r_{\rm rms}$. The reason is

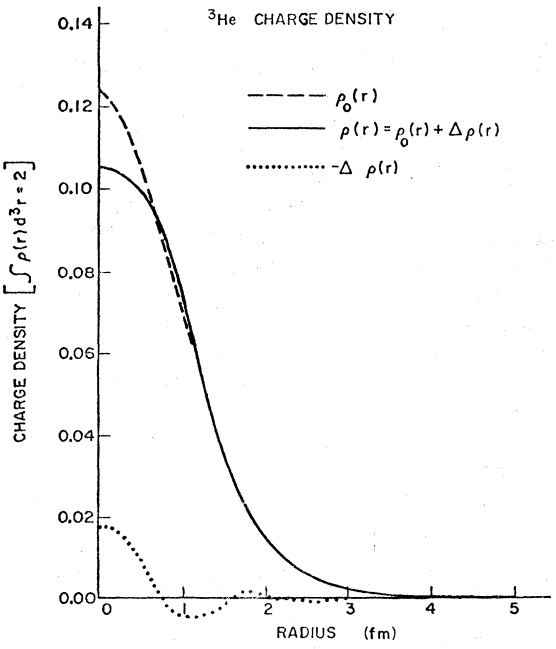

FIG. 8. ^{3}He charge distribution [Eqs. (6) and (7)].

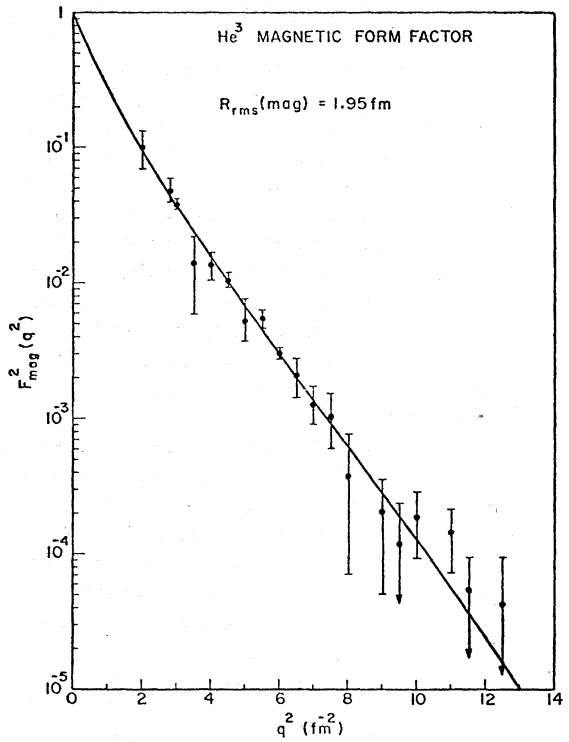

FIG. 9. ^{3}He magnetic form factor together with best fit (Eq. 6).

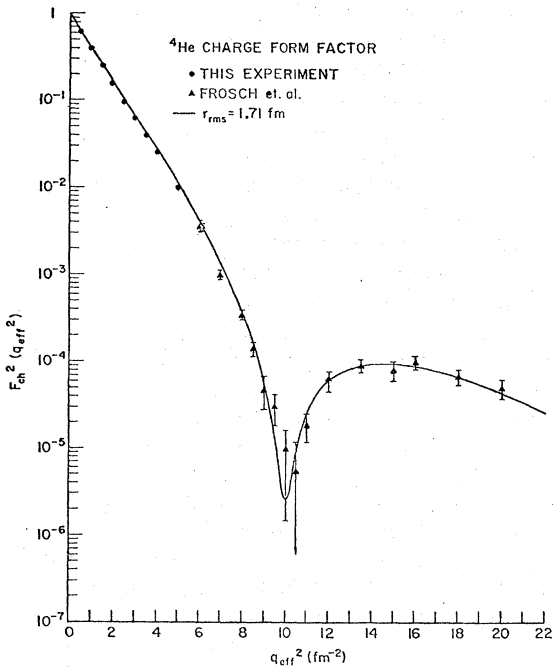

FIG. 10. ^{4}He charge form factor (for clarity only one-fifth of the new medium-q data are plotted); triangles are from Ref. 4.

that only the Fermi distribution has an exponential tail. If one smoothly adds on to the other distribution an exponential tail having a falloff corresponding to the binding energy of a proton, the value of r_{rms} increases by 0.04 fm which accounts for the difference. (For the best rms radii see Sec. IV B.)

B. Model-independent charge densities

In this section we will describe an analysis of the helium data with a method that allows a determination of $\rho(r)$ without using model densities. Under quite general assumptions a charge density together with realistic error bars can be obtained. It is desirable to derive such nearly model-independent densities, because the models couple very strongly densities at different radii. As a consequence, it is difficult to judge whether a particular feature of $\rho(r)$ is due to the model, or whether it is really required by the data. The main motivation to carry out such a "model-independent" analysis is to derive realistic error bars for $\rho(r)$; only for measured quantities accompanied by error bars can a sensible comparison with theory be made.

When determining charge densities without using models different approaches can be used. They differ by the way they deal with the limitation of the experiment to a certain maximum momentum transfer q_{max}. Because of this limitation amplitudes of the Fourier components of $\rho(r)$ having a wave length $\lambda < 2\pi/q_{max}$ are not determined.

In the approach used in Ref. 16 the density is parametrized by a sum of sine functions. The highest frequency allowed for is chosen such that the density contains no Fourier components with $\lambda < 2\pi/q_{max}$ other than the ones contained in the model density ρ_0. The resulting error bars on $\rho(r)$ consequently concern the low Fourier components of $\rho(r)$ only, and are not expected to cover the densities determined from (future) experiments going to larger q_{max}; the derived "error bars" do not have the usual meaning.

The approach of Ref. 17 is similar in the parametrization of $\rho(r)$, but differs in the treatment of the higher Fourier components. Different behaviors of the form factor in the q region not covered by experiment are assumed. For instance, upper limits for $F(q > q_{max})$ are obtained by assuming $F(q)$ to be falling exponentially with q. The upper limits are hoped to correspond to a "reasonable" behavior of $F(q)$, but it is hard to justify this extrapolation by physical arguments.

The procedure[18,19] used here makes the assumption of "reasonableness" in the quantity to be determined, in $\rho(r)$. There, a justification by phy-

sical arguments is more direct, because a comparison with theoretical densities can be made. In order to decouple the densities at different radii, the charge density is written as a sum of Gaussians (SOG), centered at different radii. The assumption mentioned above consists of permitting no structure in $\rho(r)$ narrower than a certain width Γ (full width at half maximum), i.e., not allowing the Gaussians to have a width smaller than Γ. This width, or the amount of structure in the density, is limited because the proton radial wave functions R_κ are solutions of a Schrödinger equation which strongly couples the second derivative of R_κ to the energy eigenvalue. For theoretical calculations yielding energy eigenvalues close to the experimental ones, the maximal structure in R_κ is severely limited. As a consequence, very different theoretical calculations yield practically the same value for Γ. Using this Γ to limit the fine structure of $\rho(r)$ allows the derivation of model-independent densities, i.e., densities having an error bar that includes a realistic estimate for the uncertainty due to finite q_{max}. These error bars, however, do depend on Γ, i.e., on the correctness of our present understanding of a relatively general property of nuclear wave functions.

In order to determine Γ, a number of very different theoretical densities have been fitted by SOG densities with variable Γ. We have used densities resulting from a harmonic oscillator potential, from the δ-function potential[20]; from the Hartree-Fock calculations using density-dependent forces,[21] or from the density calculated[22] by solving the Faddeev equation for realistic nucleon-nucleon interactions. Also employed was the density[23] obtained using harmonic oscillator wave functions together with short range nucleon-nucleon correlations introduced through a Jastrow factor. The values for Γ obtained from above calculations differ by ~15%, the smallest value being 1.3 fm. This value allows a fit, in the region 0–5 fm, of the densities[20-23] within a deviation of less than 0.1%. This observation gives the most direct proof that, in spite of the limitation to a given width and the choice of a Gaussian shape for the basis function, SOG densities provide enough flexibility to reproduce the amount of structure which, according to a variety of theoretical calculations, can be expected in $\rho(r)$. We therefore do expect that with SOG densities we are exploring the full range of possible densities having a physically reasonable amount of structure.

It is also assumed that all charge be located within a radius of ~6 fm. This very weak assumption is made because[19] of the relatively large spacing between data points at large momentum transfer; as a consequence, one cannot give anything but (quite low) upper limits for $\rho(r)$ for radii $r>6$ fm.

The ^{3}He data used to determine the SOG densities are the ones of Table I. For ^{4}He we have included the low-q data of Darmstadt[2] and the previous high data from Stanford,[4] thereby covering the maximum q-range experimentally explored. The statistical as well as the systematic errors of the data are taken into account. The dominant systematic error is a normalization uncertainty common to all cross sections of one set of data. For the Darmstadt data, it is ±0.8%, for the present ^{4}He data ±2%, for the ^{4}He data of Ref. 4 ±6%; for the ^{3}He data ±3% is used as the normalization uncertainty.

Figures 11 and 12 and Table IV give the extreme limits (rather than the usual $\pm\sigma$ limits) of the ^{3}He and ^{4}He charge densities. (Parameters of the SOG densities are available on request.) These limits cover systematic and statistical errors of the data as well as the lack of higher-q data. At radii $r<0.5$ fm the error bars of $\rho(r)$ are primarily due to the lack of higher-q data; at larger radii the systematic uncertainties become important.

The SOG—and model—densities agree practically everywhere within the error bars provided by the model-independent analysis. Small deviations,

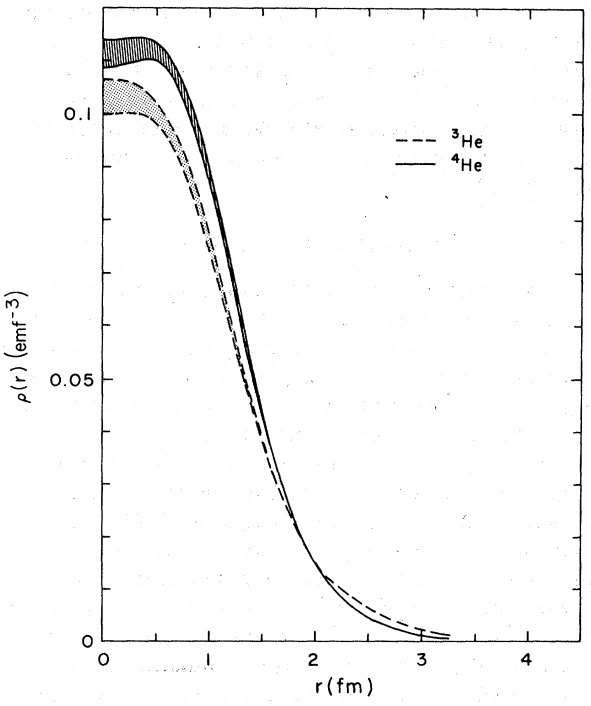

FIG. 11. ^{3,4}He model-independent charge densities. The extreme limits of $\rho(r)$ cover the statistical, systematical, as well as the completeness error of the data.

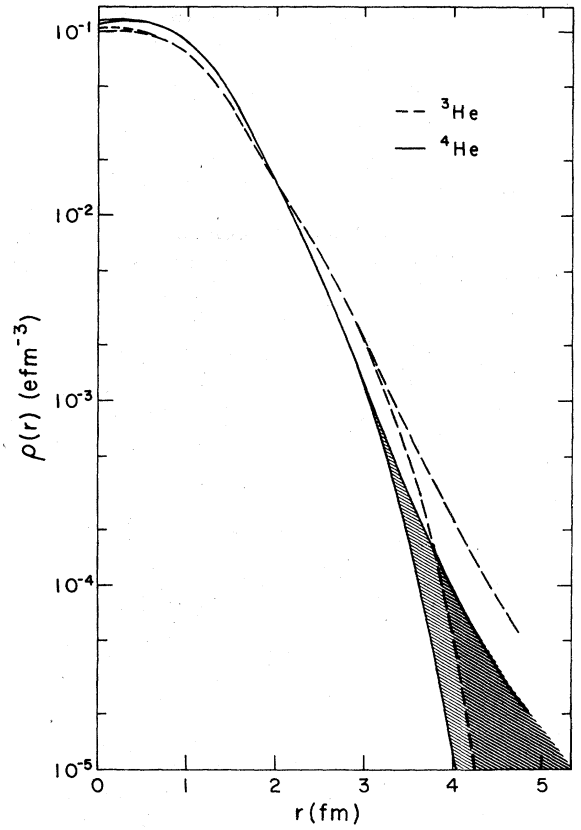

FIG. 12. See caption Fig. 11.

of at most the size of the error bar on $\rho(r)$, are due to the small flexibility of the model. Such small deviations are to be expected since the values for χ^2 are lower for the SOG—than for the model—densities. For ^{3}He(^{4}He) the χ^2 is 20(53) for 32(76) degrees of freedom; the best models give a χ^2 of 26(98).

The comparison with the ^{3}He density derived in Ref. 17 shows that the densities agree within error bars. For ^{4}He the agreement is also quite good; small deviations, at most of the size of the error bars, are due to the fact that here we analyze a more complete set of data that yields more precise information on the value of the cross section below 2 fm^{-1}.

An inspection of Fig. 11 shows that at radii $r<0.6$ fm the SOG densities produce a practically flat charge density. It is this property of $\rho(r)$ which made necessary the modification used in Eq. (7). At radii of 2–3 fm the ^{3}He density falls much more slowly than the one of ^{4}He (see Fig. 12). At large radii ($r>3$ fm) the radial dependence of both densities is compatible with the shape expected for a proton bound by the known separation energies in a nuclear potential well.[19] This difference in the large-r behavior approximately explains[6] the difference in the rms radius between ^{3}He and ^{4}He.

TABLE IV. Model-independent charge densities.

r (fm)	ρ (^{3}He) (e fm^{-3})	ρ (^{4}He) (e fm^{-3})
0	0.0997 −0.1067	0.1085 −0.1135
0.25	0.1001 −0.1058	0.1094 −0.1140
0.5	0.0986 −0.1023	0.1102 −0.1128
0.75	0.0897 −0.0933	0.1029 −0.1053
1	0.0747 −0.0776	0.0871 −0.0893
1.25	0.0557 −0.0576	0.0650 −0.0666
1.5	0.0378 −0.0393	0.0433 −0.0443
1.75	0.0242 −0.0251	0.0262 −0.0269
2	0.0152 −0.0157	0.0149 −0.0152
2.25	0.009 68−0.010 08	0.008 26−0.008 50
2.5	0.006 12−0.006 42	0.004 51−0.004 66
2.75	0.003 63−0.003 90	0.002 35−0.002 51
3	0.002 00−0.002 20	0.001 10−0.001 27
3.25	0.000 99−0.001 19	0.000 47−0.000 60
3.5	0.000 42−0.000 65	0.000 17−0.000 29
3.75	0.000 16−0.000 37	0.000 04−0.000 15
4	0.000 05−0.000 23	0.0 −0.000 09
4.25	0.0 −0.000 14	0.0 −0.000 05
4.5	0.0 −0.000 09	−0.000 03

In Fig. 13 we give the moments $M(k)=\langle r^k\rangle^{1/k}$ calculated for ^{3}He and ^{4}He. These moments are derived by using SOG densities having a width $\Gamma=1.1$ fm equaling the proton diameter. The rather precise knowledge on $\rho(r)$ at small radii is due to both the large q_{max} and the low value of the smallest form factor measured. Because $M(K)$ for small K is sensitive to the properties of $\rho(r)$ for small radii, Fig. 13 confirms that $\rho(r)$ at small radii is well determined. For the present data the minimal relative error of $M(K)$ occurs at $K\simeq -1$; this is in accordance with the large q_{max}.[19] Towards medium K the error bars $\delta M(K)$ increase, reaching $M(2)=1.844\pm0.045$ and 1.672 ± 0.025 fm for the rms radii of ^{3}He and ^{4}He, respectively. For ^{4}He the error bars of the rms radius and the higher moments are always smaller because of the additional information provided by the precise low-q data from Darmstadt.[2]

It is perhaps instructive to consider a few values for the ^{4}He rms radius as extracted from different sets of data. The Darmstadt cross sections alone give 1.64 ± 0.08 fm, the previous Stanford data[4] yield 1.74 ± 0.09 fm. The new medium-q data taken in this experiment permit a reduction in the uncertainty to 1.67 ± 0.05 fm; but only when taking all these data sets together, i.e., combining low- and high-q data, the above mentioned 1.672 ± 0.025 fm is obtained. The radii determined with models

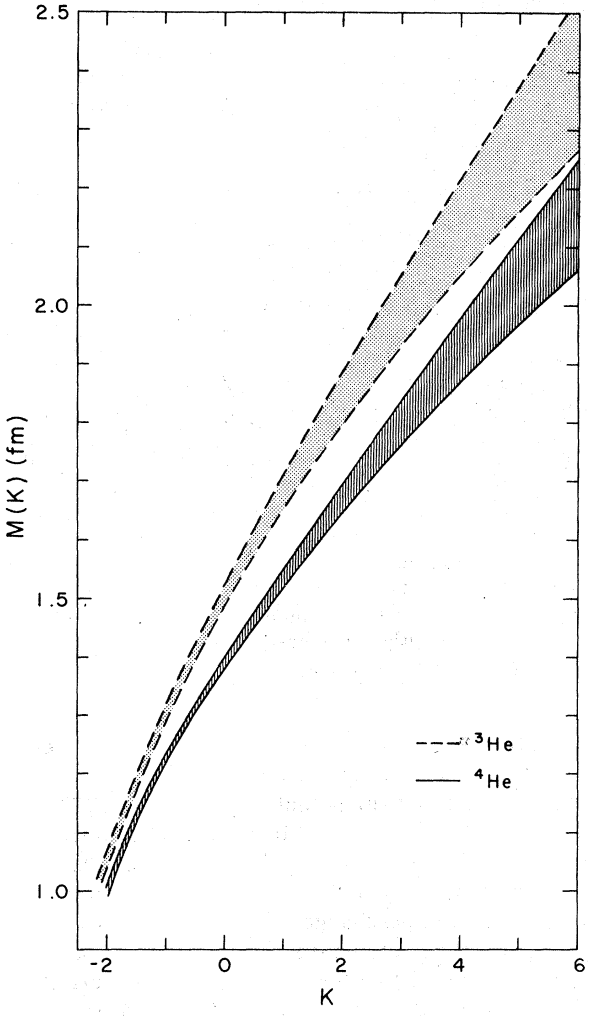

FIG. 13. Moments $\langle r^k \rangle^{1/k}$ of the ^{3,4}He charge densities (note suppressed zero).

agree with the present SOG values; their error bars, however, are generally a factor of 2 small, as a consequence of the overly restrictive conditions imposed by the model.

C. Corrections

In the analysis above the charge density has been extracted from the data by using the usual density to cross-section relation corresponding to one photon exchange and nonrelativistic nucleons. Several corrections to this simplified picture should be considered.

Intermediate excitation of the nucleus leads to an additional contribution to the elastic cross section. These so-called dispersion corrections have been calculated for ^{3}He and ^{4}He in the framework of multiple potential scattering.[24] The resulting corrections to the charge form factors are quite small; the largest relative contribution occurs in the diffraction minimum and amounts to about one-third of the experimental error bars. Correcting the data for the calculated dispersion contributions does not produce noticeable changes of $\rho(r)$. The usually practiced neglect of two photon exchange contributions is therefore justified.

When computing (e, e) cross sections from theoretical or phenomenological densities, one generally does not take into account that relativistic kinematics, rather than the usual nonrelativistic form for the electromagnetic interactions, should be used. The effect of the nonrelativistic interaction on the form factors of helium has recently been discussed.[25] In order to correct for the use of nonrelativistic kinematics, the modification of the phenomenological densities is calculated here.

The change of $\rho(r)$ obtained when applying the corrections[25] has been derived by calculating $\rho(r)$ as the Fourier transform of the corrected and uncorrected charge form factors. The resulting change in $\rho(r)$ is given in Fig. 14 for both ^{3}He and ^{4}He. Adding this $\Delta\rho(r)$ to the phenomenological densities determined above yields a density corrected for the neglect of relativistic effects.

The influence of the calculated relativistic contributions looks quite important when considering the

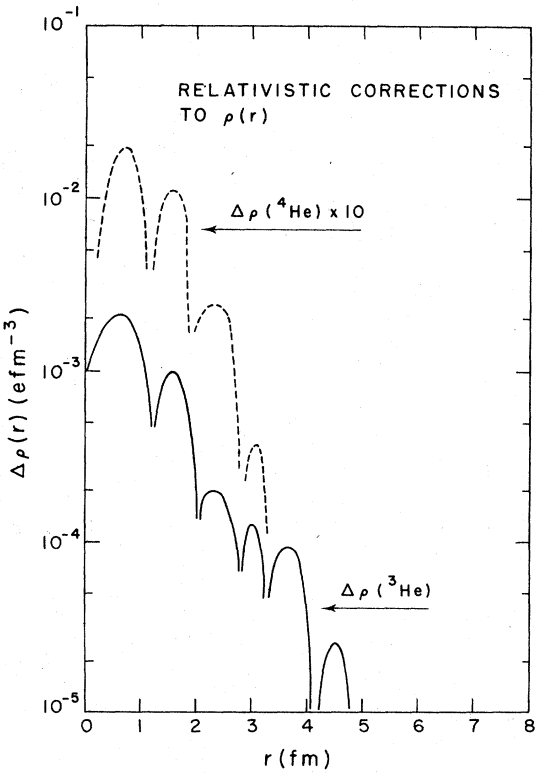

FIG. 14. Change of $\rho(r)$ due to relativistic corrections.

form factor $F(q)$. The position of the diffraction minimum, for instance, is shifted by 0.8 fm^{-2}. The corresponding change of $\rho(r)$, a rapidly oscillating function of r is quite small, however. It amounts to, at maximum, 2.5% of $\rho(r)$ for radii smaller than 3 fm. Typically, the change of $\rho(r)$ is of the order of one-half of the full error bar $\delta\rho(r)$ as determined in the previous section.

D. Point density

The flatness of the ^{3}He and ^{4}He densities at small radii is unexpected. If the charge density is simply obtained by folding the density of pointlike nucleons with the nucleon charge distribution, then, based on the available theoretical helium point densities, one would expect the charge density $\rho(r)$ to have a distinct peak at $r=0$.

In the plane wave Born approximation the folding of the point density $\rho_p(r)$ with the finite nucleon size leads to a charge form factor $F(q)$ that is the product of the body form factor $F_p(q)$ and the nucleon charge form factor $F_N(q)$:

$$F(q)=F_N(q)F_p(q)\,. \tag{11}$$

For the present application it is accurate enough to take the simple dipole form for

$$F_N(q)=(1+a^2q^2)^{-2};\quad a=0.055\ \text{fm}^{-2}\,. \tag{12}$$

If, therefore, $F_p(q)$, rather than $F(q)$, is analyzed with SOG densities, one obtains the body density of ^{3,4}He, approximately.

As discussed in a previous section for the charge density, the needed width Γ has been derived from the theoretical point densities.[20-23] We find a value of $\Gamma_p=0.85$ fm, in agreement with the expectation that the sum of Γ_p^2 and the proton diameter squared give Γ^2. The point densities, calculated in the same way as the charge densities in section B, are given in Fig. 15. The "unfolding" of the finite nucleon charge distribution leads, of course, to error bars $\delta\rho_p(r)$ which are considerably larger than for $\rho(r)$.

The most interesting observation emerging from Fig. 15 concerns the behavior of $\rho_p(r)$ at small radii. At $r<0.8$ fm an important central depression is observed. In the charge density this structure is almost completely washed out by the proton finite size. That this folding has such an important effect can be understood by considering the fact that the rms radii of the proton (0.8 fm) and ρ_p(1.45 fm) are of comparable size. Only a point density having such a depression can lead, after folding, to a charge density that is practically flat at small radii. [For smaller Γ, point densities having a central maximum can be found[26]; these densities, however, show rapidly oscillating components that are judged to be unreasonable (see Sec. IV B)].

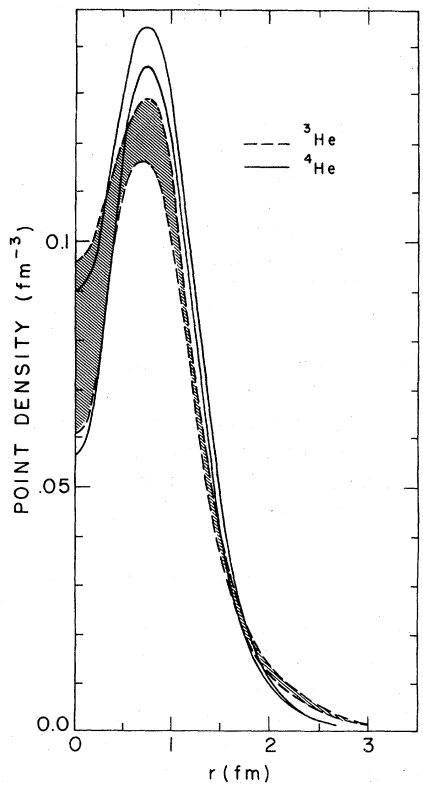

FIG. 15. Model-independent densities of pointlike protons in ^{3,4}He.

Which property of the data leads to this central depression of $\rho_p(r)$? It is the large value of the cross section beyond the diffraction minimum at $q^2\simeq 10$ fm^{-2} that requires this shape of $\rho_p(r)$. Only if the cross sections for $q^2>10$ fm^{-2} are reduced by at least a factor of 3 can the depression in the point density be made to disappear.

V. COMPARISON WITH THEORY

In this section we compare our experimental results with a number of theoretical calculations. Such a comparison is of particular interest in the case of the three-body system where very sophisticated calculations of the ground state wave functions are available. The three-body system serves as the "simplest" test case for our ability to understand nuclear properties in terms of the elementary NN interaction. Moreover, due to the unusually high values of the central densities, the three-body system, more than other nuclei, is expected to provide us with information on the short-range behavior of the NN interaction.

For the discussion of the theoretical results we first deal with the charge form factor resulting

TABLE V. Results of theoretical three-body calculations.

Type of calculation \ Reference	31 Faddeev (mom.)	29 Variational	22 Faddeev (conf.)	27 Variational	Experiment
E (^{3}H) (MeV)	−7.0	−6.7(7.3)	−7.0	−7.0(7.7)	8.48
rms radius (fm)	1.96	2.07	1.90		1.84 ± 0.03
Minimum position (fm^{-2})	13.9	12.6	14.0	12.8	11.6
$(F_{exp}{}^2/F^2)_{at\ maximum}$	3.5	2.6	3.5	10	1

from calculations based on the two-body NN interaction. A discussion of the "corrections" to be applied to this approach, such as the influence of three-body forces, off-shell effects or meson-exchange currents, follows. The magnetic form factor will be treated separately.

A. Charge distribution

Presently, there are several approaches used to obtain "exact" solutions for the three-body wave functions and binding energies on the basis of a phenomenological NN interaction. In particular, two techniques, the solution of the Faddeev equations and the variational method, have been pushed to a high degree of perfection. Since 1970 there have been a great number of theoretical calculations[27-41] attempting to fit the experimental form factors simultaneously with other three-body parameters. Here we only discuss some of the more complete calculations.

Delves and Hennell[27] perform a variational calculation using the Hamada-Johnston (HJ) and Reid soft core (RSC) potentials. Their wave function includes the symmetric, antisymmetric, and mixed symmetry S, P, and D states. The results they obtain for the binding energy, rms radius, and form factor are listed in Table V and Fig. 16. (Extrapolated energies are given in parentheses.)

These authors also point out[28] that the discrepancy in the Coulomb energy is very hard to reconcile with conceivable changes in the NN interaction. With the addition of a three-body term adjusted to fit the binding energy, their results for the form factors become worse; the diffraction minimum moves to $q^2 = 14$ fm^{-2}. The suggestion that a wider repulsive core in the NN interaction could help to fit binding energy and form factor is opposite to what is needed to fit the Coulomb energy.

Strayer and Sauer[29] perform a very complete variational calculation. Using the RSC potential, their largest harmonic oscillator basis includes 4654 states (as compared with 484 of a previous calculation[30]). These results are also shown in Fig. 16 and Table V. To test the convergence of the wave function, they compare with their results obtained using a smaller basis of 1855 states. With the decrease of the basis size they find a decrease of the binding energy, rms radius, and position of the minimum of $F(q)$ of 3, 4, and 2%, respectively. This result indicates that the wave functions are not fully converged. As compared with experiment, the binding energy, rms radius, and minimum position are reproduced to within 10%. At $q^2 = 20$ fm^{-2} the calculation form factor is $2\frac{1}{2}$ times lower than the experimental one; the secondary maximum becoming higher with in-

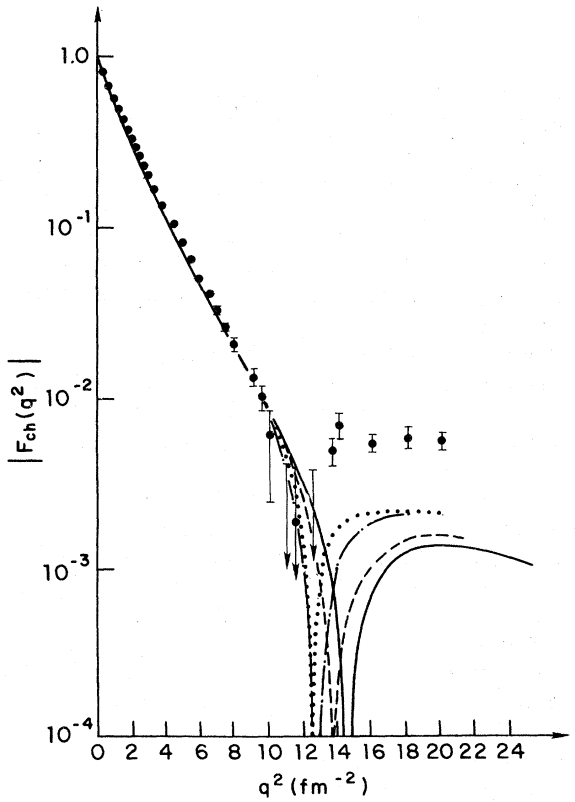

FIG. 16. Theoretical ^{3}He charge form factors: Solid curve, Ref. 33; dashed curve, Ref. 31; dotted curve, Ref. 29, and dash-dot curve, Ref. 27.

creasing basis size (by a factor of 2 for above increase), Strayer and Sauer found it probable that a fully converged wave function could yield a value close to experiment.

Brandenburg, Kim, and Tubis[31] solve the Faddeev equations in momentum space, using the RSC interaction. In particular, they have addressed themselves to the problem of convergence, and they point out that several disagreements between previous calculations are connected with cutoffs in the momentum that are too low. Their extension of the calculation of Ref. 32 uses $q_{max} = 3.1$ fm^{-1}; as compared with the previous cutoff (1.7 fm^{-1}) the binding energy increases by 0.3 MeV, and the value of F^2 in the maximum by a factor of 5. The results of their most extensive calculations are also listed in Table V and Fig. 16.

Laverne and Gignoux[22,23] solve the Faddeev equations in configuration space. As compared with working in momentum space, the *NN* potential directly rather than the *t* matrix comes in, and the energy is an eigenvalue rather than a parameter. The result of this calculation, which uses the RSC potential, truncated to the $^3S_1$, $^1S_0$, $^3D_1$, and $^3S_1$-$^3D_1$ terms, is also given in Table V and Fig. 16.

In order to test the sensitivity of three-body properties to the *NN* interaction, Laverne and Gignoux repeated their calculation using the potentials of de-Toureil and Sprung. These supersoft core potentials have little effect on the rms radius, but worsen the agreement with the experimental form factor at large q. As these authors point out, it is surprising that the binding energies obtained from such different potentials are in close mutual agreement, though far from the experimental value. Their examination of all published results shows a correlation between improvements in the form factor and a worsening of the binding energy.

Figure 16 compares some curves representative of the different approaches.[22,27,29,31] At low and medium momentum transfer, one observes reasonable agreement between the different calculations. The charge rms radius varies between 1.90 and 2.07 fm. At large q, more appreciable differences occur; the momentum transfer q_{min}^2 of the diffraction minimum varies by 1.4 fm^{-2}, and the form factor $F^2(q_{max})$ in the maximum varies by a factor of 4. The binding energy varies by 0.7 MeV, whereas the percentages of S' and D state are quite similar.

The overall agreement between these calculations, which use essentially the same input, but different techniques, is reasonably good but still indicates the presence of some artifacts of approximations that are not quite legitimate. More important differences to previous calculations can often be attributed to defects like a less complete set of wave function components, the lack of complete convergence, or the cutoff in momentum space.

The comparison of calculation and experiment reveals some clear systematic trends: the form factor at low q is too small (the rms radius being too large by 4–10%); the position of the diffraction minimum is at too large a momentum transfer, and the height of the diffraction maximum is systematically too low by a factor of 2.5–10. Also, the ^{3}H and ^{3}He nuclei are underbound by 0.8–1.8 MeV, and the Coulomb energy difference between these nuclei is about 100 keV too small.

Given the differences between the results obtained using the Reid potential, the comparison with calculations using other *NN* forces (Hamada-Johnston,[38] Gammel-Brueckner,[39] de-Toureil-Sprung,[36] OBE,[40] and Breshel-Kerman-Rouben[39,41]) does not indicate any outstanding trends. These calculations show the same shortcomings as mentioned above. At present, the calculations for the three-body system do not yet seem to provide us with additional information on the *NN* force. It would appear that, on average, the Reid soft core potential does better than the other forces, a fact that might simply be tied to the very good fit to two-body data it provides.

In order to explain the disagreement with experiment, several attempts have been made to explore additional physical effects that could contribute. These include off-shell effects, a three-body force, meson-exchange contributions, and charge asymmetry. A first possibility concerns off-shell effects in the *NN* force. The degree of freedom one has in changing the three-nucleon system properties upon arbitrary variation of off-shell properties has been investigated in several papers.[42-47] These results indicate considerable change in the form factors and they show that the binding energy can be varied by several MeV. These variations are accompanied by 5 to 10 times larger (and often much larger than desired) changes of the binding energy of nuclear matter.[42,46,48] It has been pointed out by several authors,[45,46] though, that the corresponding off-shell changes could also have a profound influence on the deuteron properties: The deuteron wave function can show nodes, and the form factor at large q can deviate very much from experiment. If, for an object as weakly bound as the deuteron, the off-shell changes become too large, they can be ruled out. The recent measurements of very-high-q data[49] on the deuteron should in this respect provide an even stronger constraint on the as-

sumed off-shell behavior.

Restricting the discussion to cases where a good fit to the (medium q) deuteron form factor has been conserved, it appears that the explored off-shell degrees of freedom change the ^{3}He binding energy by a fraction of MeV only. Moreover, the calculations of Refs. 44, 46, 47 indicate a clear correlation between the change in the binding energy and the position q_{min} of the diffraction minimum of $F_{ch}(q)$, a stronger binding leading to a larger q_{min}. At present, we therefore have no good evidence that the discrepancies in the binding energy and the form factor could simultaneously be fixed by the assumption of a suitable off-shell behavior.

Given this situation, it may seem necessary to evoke another effect not accounted for when using NN potentials derived from two-body data. ^{3}H and ^{3}He are the simplest systems that might show manifestations of a three-body force. Brayshaw[50] has recently explored the possibility of such a three-body force. After parametrizing the ^{3}H, ^{3}He form factor making some reasonable assumptions on the unknown q region (the ^{3}He form factor is known up to $q^2 \approx 8$ fm^{-2} only) and expanding the three-body wave function on a hyperspherical basis (restricted to S states), Brayshaw determines an effective local NN potential that would explain the observed form factors. A comparison with the Reid potential shows important differences at radii smaller than 1 fm; these differences are then interpreted as being caused by a three-body force. For ^{3}He, this change of the effective NN force leads to an increase of 2.7 MeV in the binding energy, a number that should be compared with the ~1.5 MeV missing in the calculations employing the Reid potential.

This calculation gets some support from a recent calculation of Shin-Non-Yang[51] who estimates the contribution of 2π exchange with an intermediary excited nucleon. The contribution of this diagram to the three-body force was calculated by using variational ^{3}H wave functions, and a contribution of 2.3 MeV to the binding energy was found. Another indication comes from the calculation of Blatt and McKellar,[52] who find for the same diagram a (larger than desired) 6 MeV/nucleon increase in the binding energy of nuclear matter.

In order to understand the discrepancies with experiment, the effect of the presence of a $\Delta(1236)$ component in the ^{3}He ground state has been investigated by Kallio *et al.*[53] Exploiting the similarity between the ΔNN and the three-nucleon d state wave function, these authors calculate the effect on the form factor for an assumed 5% Δ admixture[54] They find that the resulting change of $F(q)$ is always small and positive, shifting the diffraction minimum outward by 2–4 fm^{-2}, and decreasing the amplitude in the diffraction maximum. The resulting change in the rms radius (0.02 fm) is also small. This calculation shows that N^* admixtures (for which 5% is a safe upper limit) give a change that aggravates the disagreement with experiment.

The influence of meson-exchange currents (MEC) has also been investigated. For the same reasons as in the deuteron,[55] MEC can become important in the three-body form factor at large q; the MEC diagrams permit the sharing of the transferred momentum between two nucleons. The influence of MEC is of particular importance for the magnetic form factor and has been known for a long time.[55] For charge scattering, two recent calculations[56,57] allow us to assess the contribution of MEC. Kloet and Tjon,[56] using a pure S-state wave function calculated from the Reid potential, obtain the effect due to the "pair" diagram. They find that the diffraction minimum moves to a lower q^2 by ~3 fm^{-2}, with an increase in $F(q_{max})$ to 1.7×10^{-3}. Both these tendencies would go in the direction of improving agreement with experiment. One should add that probably these calculations considerably overestimate MEC effects. Similar calculations for the deuteron give contribution orders of magnitude too large[49] at large q. As shown by Gari and Hyuga,[66] however strong interaction vertex form factors and a smaller γ-$\pi\rho$ coupling constant greatly decrease the MEC effects.

Laverne and Gignoux[58] try to assess the importance of charge-asymmetric terms in the NN interaction. They include the Coulomb potential as well as an additional charge-asymmetric term, in order to improve on the energy difference between ^{3}H and ^{3}He. For the RSC potential, they find a small improvement in the binding energy, and an 0.08 fm improvement in the rms radius; the form factor minimum moves by 0.2 fm^{-2} only. Larger effects are found for the Gogny-Pires-de-Toureil potential which, as compared with RSC, has a smoother repulsive part.

None of the above mentioned calculations (except perhaps the one evoking three-body force) allows us to account for the (e, e) data at large q. One therefore may come back to one of the fundamental aspects in the study of the few-nucleon problem: the question of whether, due to the unusually small internucleon distances occurring in the $A = 3, 4$ nuclei, these systems do provide us with information on the short-range properties of the NN force. (In the discussion of qualitative effects we may include ^{4}He, whose form factor behavior is very similar.)

A number of studies have been carried out to

investigate the effects of a change in the short-range NN interaction; a review has been given by Ciofi degli Atti.[59] These studies are mostly carried out in the framework of the Jastrow approach which introduces in a phenomenological way a change of the wave function for small internucleon distances, with little modification of the large-distance behavior. In a number of cases, these calculations, performed mostly by using harmonic-oscillator-uncorrelated wave functions in the variational procedure, show that the high-q part of $F(q)$ is very sensitive to the short-range behavior. Basically, these calculations reproduce, through the suppression of the wave function at short internucleon distances, the central minimum that resulted from the analysis of the data in terms of a phenomenological point density (see the previous section).

B. Distribution of magnetism

The magnetic form factor has attracted less attention. In part, this is due to the less extensive ($q^2 \leq 16$ fm^{-2}) and less precise experimental data. Also, the meson-exchange processes being more important, the magnetic form factor is less useful as a test of our understanding of nuclei in terms of the pure NN interaction.

A number of calculations[27,32,34,37,41,44] for the three-body magnetic form factor seemed to produce acceptable agreement with experiment. In most cases, however, this has recently been found to be due to the neglect of the S-D interference term.[61] Including this term, as has been done in the calculation of Brandenburg, Kim, and Tubis[60] who give a complete solution of the Faddeev equations for the Reid potential, leads to the form factor shown in Fig. 17. A diffraction minimum at much too low a momentum transfer appears.

A systematic discussion of MEC diagrams contributing to the magnetic moment has been given by Chemtob and Rho.[63] For both ^{3}H and ^{3}He their calculation leads to much better agreement with experiment, and their findings are in agreement with the calculation of Refs. 61, 62, and 64. The rather complete calculation of Harper *et al.*[64] shows that MEC contribute 0.42 (0.01) magnetons to the vector (scalar) magnetic moments; these contributions account within 0.02 μ_N for the disagreement between experiment and the standard Faddeev calculations. The calculations of Ref. 61 show that the effect of MEC on the magnetic form factor considerably improves agreement with experiment. The slope of F_M^2 at medium q is closer to experiment, and the position of the diffraction minimum is increased to $\approx$11 fm^{-2}

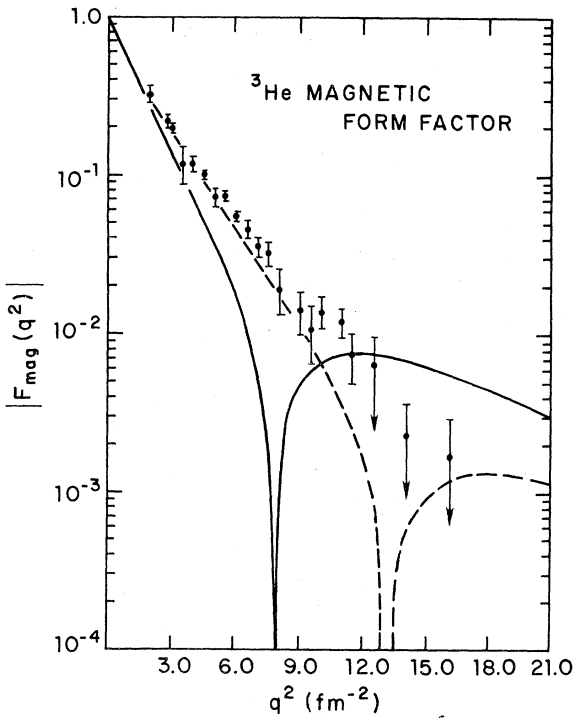

FIG. 17. ^{3}He magnetic form factor together with calculation of Ref. 60. Dashed curve without, solid curve with S/D interference term.

[above 12 fm^{-2} the experimental data are compatible with $F_M(q) = 0$].

VI. CONCLUSIONS

The investigation of the three-body system is the first step in determining if the properties of complex nuclei can be explained in terms of the basic NN interaction. Electron scattering is a fundamental tool in this quest, supplying consistent and unambiguous information. We have presented new data on the charge and magnetic form factors for ^{3}He and the charge form factor of ^{4}He. These measurements have been confirmed by the independent experiment undertaken by Bernheim *et al.*[65] at Orsay.

A number of calculations are in reasonable agreement with the experimental results for the rms radii and the low- and medium-q^2 behavior of the form factors. However, no theoretical approach has reproduced the height of the secondary maximum for ^{3}He, and the Coulomb energy and nuclear binding energies are consistently low. It may be that the approximate calculations are not yet accurate enough for direct comparison; however, the recent agreement between different methods and their approach to convergence would

tend to point to some other area for the solution. It is obvious that considerable effort will be required on questions concerning three-body forces, meson exchange, and N^* admixtures before the remaining disagreement to experiment can be resolved.

Additional experimental information is required in the following areas: The charge form factor measurements on ^{3}He and ^{4}He should be extended to yet higher q^2; the accuracy and extent of the magnetic form factor data for ^{3}He should be improved; and a program to add comparable data on ^{3}H is desirable. If advances are to be made in our understanding of the three-body system, the additional information is vital.

The authors would like to express their appreciation for the enthusiastic support of Professor Robert Hofstadter and Professor Mason Yearian during the course of the experiment. Dr. Gloria Li, Dr. Joseph Uhrhane, and Dr. George Rothbart offered considerable assistance during the data collection period. The entire staff of the Stanford High Energy Physics Laboratory were superb in the concentrated effort it took to carry this difficult experiment to completion.

---

*Work supported in part by the National Science Foundation Grant No. GP28299, the Office of Naval Research Contract No. 225(67), and the U. S. Energy Research and Development Administration Contract No. AT-(40-1)-4043.

†Supported in part by the Swiss National Science Foundation.

‡Present address: 272 Grantwood Drive, Amherst, Massachusetts 01002.

[1]H. Collard, R. Hofstadter, E. B. Hughes, A. Johansson, M. R. Yearian, R. B. Day, and R. T. Wagner, Phys. Rev. 138, B57 (1965).

[2]U. Erich, H. Frank, D. Haas, and H. Prange, Z. Phys. 208, 209 (1968).

[3]R. W. McAllister and R. Hofstadter, Phys. Rev. 102, 851 (1956); G. R. Burleson and H. W. Kendall, Nucl. Phys. 19, 68 (1960).

[4]R. F. Frosch, J. S. McCarthy, R. E. Rand, and M. R. Yearian, Phys. Rev. 160, 874 (1967).

[5]J. P. Repellin, P. Lehmann, J. LeFrançois, and D. B. Isabelle, Phys. Lett. 16, 169 (1965).

[6]J. S. McCarthy, I. Sick, R. Roy Whitney, and M. R. Yearian, Phys. Rev. Lett. 25, 884 (1970).

[7]L. R. Suelzle and M. R. Yearian, in *Proceedings of the International Conference on Nucleon Structure, at Stanford University, 1973,* edited by R. Hofstadter and L. I. Schiff (Stanford U.P., Stanford, 1964).

[8]T. Janssens, R. Hofstadter, E. B. Hughes, and M. R. Yearian, Phys. Rev. 142, 922 (1966).

[9]R. Frosch, H. Crannell, J. S. McCarthy, R. E. Rand, R. S. Safrata, L. R. Suelzle, and M. R. Yearian, Phys. Lett. 24B, 54 (1967).

[10]T. R. Fisher, D. C. Healey, D. Parks, S. Lazarus, J. S. McCarthy, and R. W. Whitney, Rev. Sci. Instrum. 41, 684 (1970).

[11]Constructed in part by Cryogenics Associates, Indianapolis, Ind.

[12]J. Wilks, *The Properties of Liquid and Solid Helium* (Clarendon, Oxford, 1967).

[13]B. T. Chertok, E. C. Jones, W. L. Bendel, and L. W. Fagg, Phys. Rev. Lett. 23, 34 (1969).

[14]L. W. Mo and Y. S. Tsai, Rev. Mod. Phys. 41, 205 (1969).

[15]G. Miller, Ph.D. dissertation, Stanford University, 1970 (unpublished).

[16]J. L. Friar and J. Negele, Nucl. Phys. A212, 93 (1973).

[17]J. Borysowicz and H. Hetherington, Phys. Rev. C 7, 2293 (1973).

[18]I. Sick, Phys. Lett. 44B, 62 (1973).

[19]I. Sick, Nucl. Phys. A218, 509 (1974).

[20]R. Frosch, Phys. Lett. 37B, 140 (1971).

[21]X. Campi, J. Martorelli, and D. W. L. Sprung, Phys. Lett. 41B, 443 (1972).

[22]A. Laverne and C. Gignoux, Nucl. Phys. A203, 597 (1973).

[23]C. Ciofi degli Atti and M. E. Grypeos, Nuovo Cimento Lett. 2, 587 (1969).

[24]V. N. Boitsov, L. A. Kondratyuk, and V. B. Kopeliovich, Yad. Fiz. 16, 515 (1972) [Sov. J. Nucl. Phys. 16, 287 (1973)].

[25]J. L. Friar, Phys. Lett. 43B, 108 (1973).

[26]I. Sick, in *Proceedings of the International Conference on Photonuclear Reactions and Applications, Asilomar, 1973,* edited by B. L. Berman (Lawrence Livermore Laboratory, Univ. of California, 1973), p. 8A5.

[27]L. M. Delves and M. A. Hennell, Nucl. Phys. A168, 347 (1971); A246, 490 (1975).

[28]M. A. Hennell and L. M. Delves, Phys. Lett. 34B, 195 (1971).

[29]M. R. Strayer and P. U. Sauer, Nucl. Phys. A231, 1 (1974).

[30]A. D. Jackson, A. Lande, and P. U. Sauer, Nucl. Phys. A156, 1 (1970).

[31]R. A. Brandenburg, Y. E. Kim, and A. Tubis, Phys. Rev. C 12, 1368 (1975).

[32]E. P. Harper, Y. E. Kim, and A. Tubis, Phys. Rev. Lett. 28, 1533 (1972).

[33]A. Laverne and C. Gignoux, Phys. Rev. Lett. 29, 436 (1972).

[34]J. A. Tjon, B. F. Gibson, and J. S. O'Connell, Phys. Rev. Lett. 25, 540 (1970).

[35]R. A. Malfliet and J. A. Tjon, Nucl. Phys. A127, 161 (1969).

[36]R. A. Malfliet and J. A. Tjon, Phys. Lett. 29B, 391 (1969).

[37]S. N. Yang and A. D. Jackson, Phys. Lett. 36B, 1 (1971).

[38]E. Hadjimichael, E. Harms, and V. Newton, Phys. Lett. 40B, 61 (1972).

[39]M. McMillan, Phys. Lett. 40B, 437 (1972).

[40]E. Harper, Phys. Rev. Lett. 34, 677 (1975).

[41]R. A. Malfliet and J. A. Tjon, Phys. Lett. 35B, 487

(1971).
[42]Y. E. Kim and A. Tubis, Phys. Lett. 38B, 354 (1972).
[43]M. M. Hoenig, Phys. Rev. C 3, 1118 (1971).
[44]P. U. Sauer and J. A. Tjon, Nucl. Phys. A216, 541 (1973).
[45]N. J. McGurk and H. De Groot, Nucl. Phys. A231, 233 (1974).
[46]M. I. Haftel, Phys. Rev. C 7, 80 (1973).
[47]E. P. Harper, Y. E. Kim and A. Tubis, Phys. Rev. C 6, 1601 (1972).
[48]M. I. Haftel and F. Tabakin, Phys. Rev. C 3, 921 (1971).
[49]R. G. Arnold, B. T. Chertok, E. B. Dally, A. Grigorian, C. L. Jordan, W. P. Schütz, R. Zdarko, F. Martin, and B. A. Mecking, Phys. Rev. Lett. 35, 776 (1975).
[50]D. D. Brayshaw, Phys. Rev. C 7, 1731 (1973).
[51]Shin-Non-Yang, Phys. Rev. C 10, 2067 (1974).
[52]D. W. E. Blatt and B. H. J. McKellar, Phys. Rev. C 11, 614 (1975).
[53]A. J. Kallio, R. Toropainen, A. M. Green, and T. Kouki, Nucl. Phys. 231, 77 (1974).
[54]A. M. Green and T. H. Schucan, Nucl. Phys. A188, 289 (1972).
[55]F. Villars, Helv. Phys. Acta 20, 476 (1947).
[56]W. M. Kloet and J. A. Tjon, Phys. Lett. 49B, 419 (1974).
[57]E. Hadjimichael, in *Symposium on Interaction Studies in Nuclei*, proceedings of the 1975 Mainz symposium, edited by H. Jochim and B. Ziegler (North-Holland, Amsterdam, 1975).
[58]A. Laverne and C. Gignoux, in *Proceedings of the International Conference on Few Particle Problems in Nuclear Physics, Los Angeles, 1972,* edited by I. Slaus (North-Holland, Amsterdam, 1973), p. 411.
[59]C. Ciofi degli Atti, in *The Nuclear Many Body Problem,* edited by C. Ciofi degli Atti and F. Calogero (Editrice Compositori, Bologna, 1973).
[60]R. A. Brandenburg, Y. E. Kim, and A. Tubis, Phys. Rev. Lett. 32, 1325 (1974).
[61]A. Barroso and E. Hadjimichael, Nucl. Phys. A238, 422 (1975).
[62]W. M. Kloet and J. A. Tjon, Nucl. Phys. A176, 481 (1971).
[63]M. Chemtob and M. Rho, Nucl. Phys. A163, 1 (1971).
[64]E. P. Harper, Y. E. Kim, A. Tubis, and M. Rho, Phys. Lett. 40B, 533 (1972).
[65]M. Bernheim, D. Blum, W. McGill, R. Riskalla, C. Trail, T. Stovall, and D. Vinciguerra, Nuovo Cimento Lett. 5, 431 (1972).
[66]M. Gari and M. Hyuga, Phys. Rev. Lett. 36, 345 (1976).